2023

Toward systems-informed models for biologics disposition: covariates of the abundance of the neonatal Fc Receptor (FcRn) in human tissues and implications for pharmacokinetic modelling

Jill Barber

Zubida M. Al-Majdoub

Narciso Couto

Martyn Howard

Yasmine Elmorsi

See next page for additional authors

Citation/Publisher Attribution

Barber, J., Al-Majdoub, Z. M., Couto, N., Howard, M., Elmorsi, Y., Scotcher, D.,...Achour, B. (2023). Toward systems-informed models for biologics disposition: covariates of the abundance of the neonatal Fc Receptor (FcRn) in human tissues and implications for pharmacokinetic modelling. *European Journal of Pharmaceutical Sciences, 182*, 106375. https://doi.org/10.1016/j.ejps.2023.106375
Available at: https://doi.org/10.1016/j.ejps.2023.106375

Toward systems-informed models for biologics disposition: covariates of the abundance of the neonatal Fc Receptor (FcRn) in human tissues and implications for pharmacokinetic modelling

Authors

Jill Barber, Zubida M. Al-Majdoub, Narciso Couto, Martyn Howard, Yasmine Elmorsi, Daniel Scotcher, Naved Alizai, Saskia de Wildt, Felix Stader, Armin Sepp, Amin Rostami-Hodjegan, and Brahim Achour

Creative Commons License

This work is licensed under a Creative Commons Attribution-Noncommercial-No Derivative Works 4.0 License.

European Journal of Pharmaceutical Sciences 182 (2023) 106375

Contents lists available at ScienceDirect

European Journal of Pharmaceutical Sciences

journal homepage: www.elsevier.com/locate/ejps

Toward systems-informed models for biologics disposition: covariates of the abundance of the neonatal Fc Receptor (FcRn) in human tissues and implications for pharmacokinetic modelling

Jill Barber [a], Zubida M. Al-Majdoub [a], Narciso Couto [a], Martyn Howard [a], Yasmine Elmorsi [a], Daniel Scotcher [a], Naved Alizai [b], Saskia de Wildt [c], Felix Stader [d], Armin Sepp [d], Amin Rostami-Hodjegan [a,d], Brahim Achour [e,*]

[a] Centre for Applied Pharmacokinetic Research, the University of Manchester, Manchester, United Kingdom
[b] Leeds Teaching Hospitals, Leeds, United Kingdom
[c] Radboud University Medical Center, Radboud University, Nijmegen, the Netherlands
[d] Certara UK Ltd. (Simcyp Division), Sheffield, United Kingdom
[e] Department of Biomedical and Pharmaceutical Sciences, College of Pharmacy, the University of Rhode Island, 495A Avedisian Hall, 7 Greenhouse Road, Kingston, RI 02881, United States

ARTICLE INFO

Keywords:
Systems pharmacology
Biologics
FcRn
Pharmacokinetics
pharmacodynamics

ABSTRACT

Biologics are a fast-growing therapeutic class, with intertwined pharmacokinetics and pharmacodynamics, affected by the abundance and function of the FcRn receptor. While many investigators assume adequacy of classical models, such as allometry, for pharmacokinetic characterization of biologics, advocates of physiologically-based pharmacokinetics (PBPK) propose consideration of known systems parameters that affect the fate of biologics to enable *a priori* predictions, which go beyond allometry. The aim of this study was to deploy a systems-informed modelling approach to predict the disposition of Fc-containing biologics. We used global proteomics to quantify the FcRn receptor [p51 and β_2-microglobulin (B2M) subunits] in 167 samples of human tissue (liver, intestine, kidney and skin) and assessed covariates of its expression. FcRn p51 subunit was highest in liver relative to other tissues, and B2M was 1–2 orders of magnitude more abundant than FcRn p51 across all sets. There were no sex-related differences, while higher expression was confirmed in neonate liver compared with adult liver. Trends of expression in liver and kidney indicated a moderate effect of body mass index, which should be confirmed in a larger sample size. Expression of FcRn p51 subunit was approximately 2-fold lower in histologically normal liver tissue adjacent to cancer compared with healthy liver. FcRn mRNA in plasma-derived exosomes correlated moderately with protein abundance in matching liver tissue, opening the possibility of use as a potential clinical tool. Predicted effects of trends in FcRn abundance in healthy and disease (cancer and psoriasis) populations using trastuzumab and efalizumab PBPK models were in line with clinical observations, and global sensitivity analysis revealed endogenous IgG plasma concentration and tissue FcRn abundance as key systems parameters influencing exposure to Fc-conjugated biologics.

1. Introduction

Incorporation of patient characterization for variations in drug metabolism and transport is an established practice in the arena of small molecule drug development. However, the nature of the covariates used to define a patient (the easiest ones to measure, such as body size or age, compared with those with a mechanistic rationale, such as the genotype or phenotype of relevant enzymes and transporters) has changed over the last two decades (Rostami-Hodjegan and Achour, 2022). Moreover, as predictive modelling platforms within the framework of systems

Abbreviations: Fc, fraction crystallizable; FcRn, neonatal Fc receptor; IgG, immunoglobulin gamma; LC-MS/MS, liquid chromatography-tandem mass spectrometry; PBPK, physiologically based pharmacokinetics; PK, pharmacokinetics; PD, pharmacodynamics; QSP, quantitative systems pharmacology; TMDD, target-mediated drug disposition.

* Corresponding author.
E-mail address: achour@uri.edu (B. Achour).

https://doi.org/10.1016/j.ejps.2023.106375
Received 15 October 2022; Received in revised form 21 December 2022; Accepted 3 January 2023
Available online 7 January 2023

pharmacology have become more popular, expectations regarding the identification and quantification of the impact of influential covariates on drug kinetics have shifted from retrospective (post-hoc) data analysis, using tools such as population pharmacokinetics, to *a priori* predictions of effects before conducting any clinical studies. Hence, this creates the possibility of moving the focus from 'typical' representation of patients in clinical studies to the inclusion of sub-sets of patients in early stages when possible. The latter is advocated by regulatory agencies who have encouraged widening the recruitment criteria in drug development to provide information on the fate of drugs beyond what is known in a 'typical patient'. Two recent Guidance for the Industry documents issued by the US Food and Drug Administration (FDA) related to enhancing the diversity of clinical trial populations (FDA, 2020) and improving enrolment of participants from underrepresented racial and ethnic subpopulations in clinical trials (FDA, TM 2022) are typical examples of such attempts.

Against this backdrop, modelling the kinetics of large molecules (commonly referred to as biologics) has not made the same level of progress from empirical or allometry-based approaches to more mechanistic physiologically-based pharmacokinetic (PBPK) models. Advocates of allometry-based methods rely on subsequent clinical studies to inform changes in kinetics instead of attempting to include physiological and biological data from patients into the models based on knowledge of the interaction between the new drug and its targets using *in vitro* systems. Considering that biologics are a rapidly expanding class of therapeutic modalities and that they have opened new treatment avenues for multiple diseases, such as cancer, rheumatoid arthritis, Crohn's disease and psoriasis (Dostalek et al., 2013), the added value of shifting to PBPK models becomes more evident.

Biotherapeutics include monoclonal antibodies (mAb), recombinant and fusion proteins, antibody fragments, antibody-drug conjugates and therapeutic peptides (Shi, 2014). As of 2021, there were more than 50 approved antibodies and 60 approved peptides in use in different therapeutic applications, with over 700 additional biotherapeutics in the development pipeline (Lawrence et al., 2021). Unlike most small molecule drugs, biologics are confined to extracellular space, with tissue absorption predominantly driven by paracellular filtration/diffusion-mediated extravasation, while elimination pathways are shared with those of endogenous proteins (Dostalek et al., 2013; Shi, 2014). As a result, the factors impacting the pharmacokinetic properties of biologics are different from those of typical small molecule drugs.

The pharmacokinetics of mAbs and Fc-conjugated biologics is heavily affected by the function of the neonatal Fc receptor (FcRn), found in many tissues including the liver, muscles, skin, intestine and kidneys (Xiao, 2012; Shi, 2014). Arguably, the name FcRn is a historical misnomer (Pyzik et al., 2019) that originated from the early discovery of its involvement in transfer of immunoglobulin G (IgG) from mother to fetus (via the placenta), and later, to the new-born infant (via the intestine), a process which confers humoral immunity in the early stages of life (Simister and Rees, 1985; Story et al., 1994). More recent evidence demonstrated that this receptor is expressed throughout life (Spiekermann et al., 2002), with the main function of rescuing macropinocytosed IgG and albumin from lysosomal degradation, thus extending their plasma half-lives (Roopenian and Akilesh, 2007). Through the same mechanisms, FcRn is one of the main determinants of exposure to Fc-containing therapeutic proteins (Dostalek et al., 2013; Chang et al., 2021).

Structurally, FcRn consists of two subunits, p51 and β2-microglobulin (B2M, p14), which bind non-covalently to form a major histocompatibility complex (MHC) class I-like heterodimer (Burmeister et al., 1994). Unlike MHC-I molecules, this complex is not directly involved in antigen presentation (Story et al., 1994; Pyzik et al., 2019). B2M is also part of other MHC-I molecules, and therefore, it is ubiquitously expressed throughout the body (Burmeister et al., 1994; Story et al., 1994), while FcRn is expressed mainly in endothelial and epithelial cells in tissues as well as immune cells, especially those of monocytic lineage (Pyzik et al., 2019).

Targeted mass spectrometry (MS) based proteomics was employed to measure the abundance of FcRn in two previous studies (Fan et al., 2019; Qiu and Wang, 2020). The first (Fan et al., 2019) quantified FcRn p51 subunit in 14 tissues from five donors, and the second (Qiu and Wang, 2020) quantified both subunits in liver samples from 39 donors. To build on these reports, we analyzed global proteomic datasets (from 167 samples) generated previously in our laboratory (Couto et al., 2019, 2021; Achour et al., 2021; Al-Majdoub et al., 2020, 2021a) with the aim of creating a quantitative distribution profile of the FcRn receptor across four tissues (adult liver, pediatric liver, kidneys, intestine and skin) from healthy and diseased cohorts. The data were generated in the same laboratory using similar techniques, and therefore the same data analysis strategy was applied to allow head-to-head comparison and consistent expression profiles to be drawn. Further, implications of such data for the prediction of mAb disposition and disease effects were assessed using the Simcyp population PBPK simulator.

2. Materials and methods

2.1. Human sample sets

Eight sample sets, making 167 samples in total, were processed and analyzed by LC-MS during the period 2016–2019, as detailed previously (Al-Majdoub et al., 2020). Samples were opportunistic, collected either as surgical surplus or postmortem specimens. For clarity, the liver sample sets are designated in this study as adult liver sets 1 and 2 and pediatric liver sets 1, 2 and 3. Ethics approval was obtained and tissue samples were collected and processed as described previously for adult liver set 2 ($n = 29$), intestine ($n = 16$), kidney ($n = 20$) and skin ($n = 6$) (Scotcher et al., 2017; Couto et al., 2020, 2021; Achour et al., 2021; Al-Majdoub et al., 2021). Adult liver membrane fractions (adult liver set 1, $n = 27$) were obtained from Pfizer (Groton, USA) (Couto et al., 2019). Pediatric liver set 1 was made up from tissue samples ($n = 8$) provided by Invitron (Monmouth, UK) and individual fractions ($n = 12$) from XenoTech (Kansas, USA). Pediatric liver set 2 consisted of tissue samples obtained from Erasmus University Medical center (Leiden, The Netherlands). Pediatric liver set 3 (biliary atresia set, $n = 25$) were obtained from Ethical Tissue University of Bradford Biobank with generic ethics approval 07/H1306/98 and 17/YH/0086. Samples were collected either surgically (skin, intestine, kidney, adult liver set 2, pediatric liver set 3) or postmortem (adult liver set 1, pediatric liver sets 1 and 2). Tissue samples from pediatric sets (1 and 2) were categorized based on the European Medicines Agency (EMA) recommendations as: fetal ($n = 5$), neonates (0–1 month, $n = 15$), infants (>1 month–23 months, $n = 9$), children (2 years–11 years, $n = 11$), adolescents (12 years–17 years, $n = 3$). In addition, one liver sample from pediatric liver set 1 was collected from an 18 year-old donor (data for this sample were allocated to the adult age group in data analysis). A summary of the characteristics of the sample sets is presented in Table 1, and demographic and clinical information for each set is included in Tables S1–8.

2.2. Sample preparation for proteomics

Methods used for protein fraction preparation from adult livers, pediatric livers, kidney, intestine and skin were described previously (Scotcher et al., 2017; Couto et al., 2020, 2021; Achour et al., 2021). Liver and kidney samples were processed to total membrane fractions, intestine samples were processed to mucosal fractions, and skin samples were prepared as S9 (post-mitochondrial) fractions. Sample preparation for proteomics of all sets followed filter-aided sample preparation (FASP), with several modifications (Wiśniewski et al., 2009; Al Feteisi et al., 2018). Solubilization of proteins used sodium deoxycholate (10% w/v), and digestion was based on a multi-protease strategy, employing endopeptidase Lys-C, followed by trypsin (Russell et al., 2013; Al-Majdoub et al., 2014). Protein fractions of adult liver set 2, intestine, and

Table 1
Summary of the characteristics of the sample sets used in this study.

Sample set	Disease cohort [a]	Sex [a]	Age	Ethnicity [a]	Tissue	Extracted fraction	n
Adult liver set 1	Healthy	M (15), F (12)	27–66 years	White (25), Black (1), Hispanic (1)	Liver parenchyma	Total membrane fraction/microsomes	27
Adult liver set 2	Hepatocellular carcinoma (3), gallbladder cancer (1), colorectal cancer liver metastasis (25)	M (16), F (13)	44–85 years	White (25), - [b] (4)	Liver parenchyma (histologically normal tissue)	Total membrane fraction/microsomes	29
Pediatric liver set 1	Healthy	M (13), F (6), - [b] (1)	13 days–18 years	White (10), Black (2), Asian (1), - [b] (7)	Liver parenchyma	Total membrane fraction/microsomes	20
Pediatric liver set 2	Different cohorts	M (10), F (13), - [b] (1)	Fetal–7 years	White (16), - [b] (8)	Liver parenchyma	Total membrane fraction/microsomes	24
Pediatric liver set 3	Biliary atresia	M (12), F (13)	2 weeks–5 months	White (17), South Asian (6), Chinese (1), Black (1), - [b] (1)	Liver parenchyma	Total membrane fraction/microsomes	25
Small intestine	Ischemia (2) or no disease (2)	M (3), F (1)	29–66 years	- [b] (4)	Jejunum mucosa	Mucosal fraction	4
	Colon cancer (5), Crohn's disease (3), ischemia (1) or no disease (3)	M (9), F (3)	17–80 years	- [b] (12)	Ileum mucosa	Mucosal fraction	12
Kidney	Primary kidney cancer	M (16), F (4)	43–83 years	White (8), - [b] (12)	Kidney cortex (histologically normal tissue)	Total membrane fraction/microsomes	20
Skin	Healthy	M (1), F (4)	27–56 years	White (5), Asian (1)	Skin	Post-mitochondrial fraction	6

[a] In parentheses are the numbers of samples in each category
[b] data not available. Abbreviations: M, male; F, female

kidney samples were spiked with stable isotope-labeled QconCATs [MetCAT and/or TransCAT (Russell et al., 2013)], whereas pediatric livers, adult liver set 1 and skin samples were mixed with exogenous protein standards (bovine serum albumin, horse myoglobin, and/or yeast aldehyde dehydrogenase) at known concentrations.

2.3. Mass spectrometry data acquisition and analysis

Sample sets were analyzed with MS-based proteomics using two LC-MS/MS platforms, Orbitrap Elite and Q Exactive HF (Thermo Fischer Scientific, Bremen, Germany), as previously detailed (Couto et al., 2020, 2021; Achour et al., 2021; Al-Majdoub et al., 2021a). Data analysis was performed using MaxQuant version 1.6.7.0 (Max Planck Institute, Martinsried, Germany) against a customized human proteome database [UniprotKB proteome UP000005640, containing 71,790 sequences (accessed Oct 2019), in addition to five QconCAT sequences and four standard protein sequences (bovine serum albumin, bovine cytochrome c, horse myoglobin and yeast aldehyde dehydrogenase)]. The search applied the following settings: 5 ppm precursor mass tolerance, 0.5 Dalton fragment mass tolerance, cysteine carbamidomethylation as a fixed modification, methionine oxidation as a variable modification, false discovery rate of 1%, and up to one missed cleavage was accommodated with trypsin/P digestion. Evidence files were used for data analysis. For consistency across samples sets, quantification of FcRn was performed using the total protein approach (TPA) (Wiśniewski et al., 2014), with minor modifications (Al-Majdoub et al., 2020). This approach applies the ratio of the MS signal intensity arising from an individual protein to the total signal intensity of the sample and converts the ratio to a concentration using the molecular mass of the protein. This affords quantitative estimates of protein abundance and comparison across sample sets or conditions (Vasilogianni et al., 2022).

2.4. Extraction of plasma exosomes and RNA sequencing

Plasma ($n = 29$) was collected from donors of liver set 2 prior to surgical resection. Exosomes were extracted from plasma using polymer-assisted precipitation (ExoQuick, System Biosciences, Palo Alto, CA) and visualized with transmission electron microscopy (Tecnai 12 Biotwin microscope, FEI Ltd., Cambridge, UK). Total RNA was extracted from exosomes (MagMax cell-free total nucleic acid isolation kit, Thermo Fisher Scientific, Austin, TX) and analysed using AmpliSeq based RNA sequencing on a NovaSeq 6000 platform with 2 × 150 bp paired-end reads (Illumina, Cambridge, UK), as detailed previously (Achour et al., 2021, 2022). Sequencing data analysis was done with RNA Amplicon App 2.0.1 (Illumina), with alignment using the Burrows Wheeler Aligner and differential expression analysis using DESeq2. Data for FCGRT gene expression (the gene that encodes FcRn) were extracted and normalized to total exosomal RNA from each sample.

2.5. Statistical analysis

Statistical analysis was performed using Microsoft Excel 2016 and GraphPad Prism 9.1.2 (GraphPad Software, La Jolla, CA). Data were expressed as mean, standard deviation (SD), coefficient of variation (CV), geometric mean, range and median. Sex-related differences were assessed in adult (liver, kidney and intestine) datasets using unpaired *t*-test. Age-related differences in abundance were assessed for liver samples by amalgamating data from four sets (adult sets 1 and 2 and pediatric sets 1 and 2) based on EMA age classification, as detailed above. Differences in these groups were tested by one-way analysis of variance (ANOVA). Post-hoc unpaired *t*-test (with Welch's correction for unequal variance) was used for pairwise comparison (Bonferroni correction of the cut-off p-value of 0.05 was performed where applicable). The effect of age after maturity was assessed by ANOVA and subsequent pairwise *t*-tests across age groups (10-year intervals). The effect of smoking and alcohol use by the adult liver and kidney donors was tested using unpaired *t*-test. Correlation of expression between FcRn subunits in each set of samples and between FcRn abundance in liver tissue and levels in matching plasma was assessed using Spearman's correlation test (Rs). Graphs were generated using Microsoft Excel 2016, Microsoft PowerPoint 2016 and GraphPad Prism 9.1.2.

2.6. Modelling the impact of FcRn abundance on mAb disposition

The generated abundance data, expressed in pmol/mg protein (Table S9), were scaled to tissue abundance, expressed in pmol/g tissue (Table S10), by multiplication with fraction-to-tissue scalars [microsomal protein per gram liver (MPPGL), microsomal protein per gram kidney (MPPGK), mucosal protein per gram intestine, S9 protein per gram skin]. The measured FcRn abundance values were applied in a minimal

PBPK model within the Simcyp Simulator (V21 R1, Certara, Sheffield, UK) to assess differences in disposition of trastuzumab and efalizumab (Li et al., 2014; Chetty et al., 2015). Changes in total endosomal FcRn content were calculated using Eq. (1) (based on measured abundance of FcRn p51 subunit), and target mediated drug disposition (TMDD) was considered. A summary of model settings is included in Table S11.

$$Total\ endosomal\ FcRn\ (\mu M) = \sum \frac{tissue\ FcRn\ (pmol/g)\ \times tissue\ mass\ (g)\ \times\ 10^{-6}}{Volume\ of\ endosomal\ space\ (L)} \quad (1)$$

For trastuzumab, simulations were conducted using virtual Healthy Volunteers and a Cancer population (10 trials x 10 subjects; 20–50 years old and 1:1 female-to-male ratio) after a single IV infusion (6 mg/kg). For efalizumab, simulations were conducted using a Psoriasis population (10 trials x 10 subjects; 20–50 years old and 1:1 female-to-male ratio) after a single IV infusion (10 mg/kg). The monitored endpoint was the systemic mAb concentration, while comparisons focused on AUC and $t_{1/2}$ after IV administration. The predicted elimination $t_{1/2}$ was calculated using averaged data from the post-distribution phase. Predictions were assessed against published clinical data for trastuzumab (Wynne et al., 2013) and efalizumab (Bauer et al., 1999).

2.7. Global sensitivity analysis (GSA)

The impact of altered FcRn abundance in combination with endogenous IgG plasma concentration, total lymph flow, and central lymph node volume on mAb exposure (AUC) was investigated by global sensitivity analysis (GSA) within the Simcyp Simulator. A minimal PBPK model for IgG without target binding (Li et al., 2014), informed by the implemented North European Caucasian population, was used for GSA analysis. The literature was analysed for physiologically plausible boundaries in relation to the investigated systems parameters (FcRn abundance, IgG plasma concentration, total lymph flow rate, central

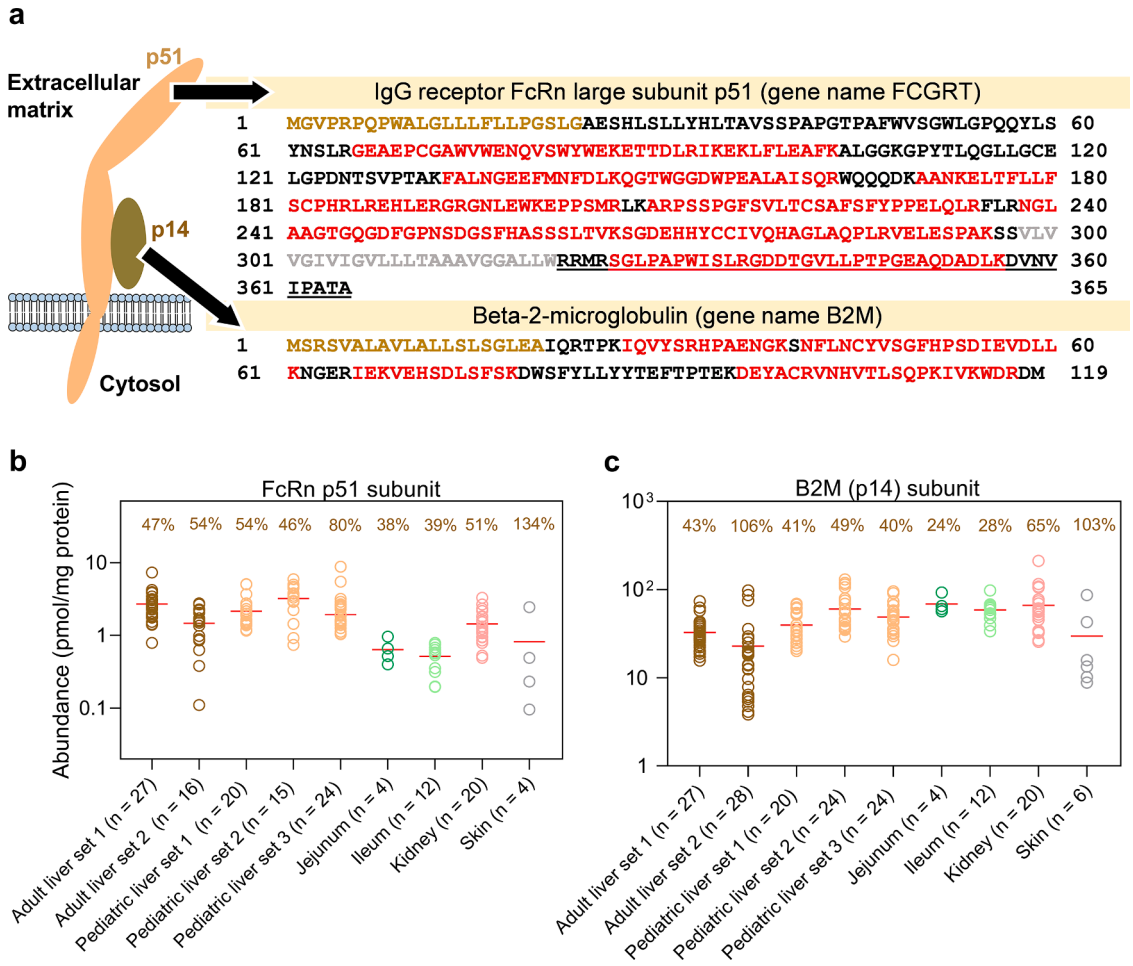

Fig. 1. Structure and quantification of the neonatal Fc receptor subunits p51 and B2M. Schematic representation of the structure and topology of FcRn subunits (**a**). The protein sequences are annotated for peptides detected by LC-MS in this study (in red), signal peptides (orange), trans-membrane chains (gray), and intracellular/cytosolic domain (underlined). B2M is bound non-covalently to the FcRn p51 on the extracellular surface of the cell membrane. The quantitative distribution of FcRn p51 (**b**) and B2M (**c**) subunits in liver (adult and pediatric), small intestine (jejunum and ileum), kidney cortex and skin reflected higher levels of B2M than FcRn p51 across all tissues. In panels **b** and **c**, individual levels and the mean (red bars) are shown with the coefficient of variability for each tissue (inter-individual variability) presented as a percentage above each set. Units are pmol per mg membrane protein (liver and kidney), pmol per mg mucosal protein (intestine) or pmol per mg post-mitochondrial supernatant protein (skin). IgG, immunoglobulin G.

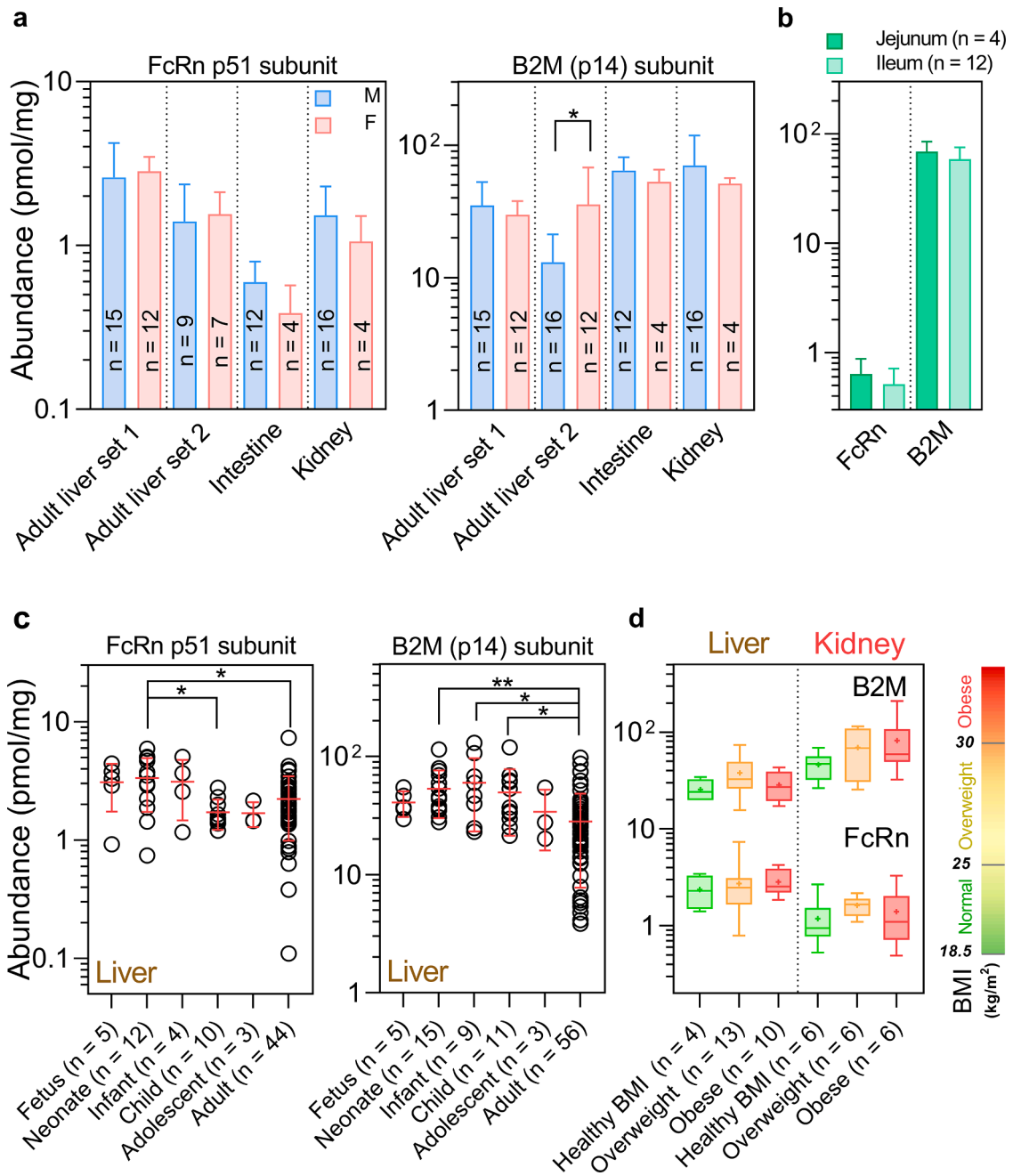

Fig. 2. Covariates of protein expression of FcRn subunits p51 and B2M in three tissues. The variables assessed are sex (**a**), intestinal anatomical region (**b**), age (**c**) and body mass index, BMI (**d**). Sex did not affect the expression of FcRn in liver, intestine and kidney (**a**). There were no differences in FcRn abundance between jejunum and ileum (**b**). Binning expression data into developmental age groups [EMA categories: fetal, neonates (0–1 month), infants (>1 month–23 months), children (2 years–11 years), adolescents (12 years–17 years), adults (18 years and over)] showed an ontogeny-related decline in FcRn abundance with age until adulthood (**c**). An overall rise in abundance of FcRn p51 and B2M proteins in liver and kidney was observed with increasing BMI (**d**). Units of abundance are pmol per mg membrane protein (liver and kidney), pmol per mg mucosal protein (intestine) or pmol per mg post-mitochondrial supernatant protein (skin). In panels **a, b** and **c**, abundance data are presented as means and error bars represent standard deviation (SD) values. In panel **a**, M, male; F, female; $^{*}p < 0.05$ (*t*-test). In panel **d**, the whiskers reflect the ranges, the boxes reflect the 25th and 75th percentiles, the lines are the medians, and the + signs are the means. The scale inset represents BMI categories (normal BMI: 18.5 – 25, overweight: 25–30, obese: >30 kg/m^2). In panel **c**, p-value cut-offs were Bonferroni-corrected in post-hoc tests to: $^{*}p < 0.01$; $^{**}p < 0.002$.

lymph node volume). IgG concentration varied between 27.9 and 148.3 μM in 460 white individuals, aged 18 to 92 years (Gonzalez-Quintela et al., 2008). FcRn abundance ranges in five subjects (14 tissues) were utilized (Fan et al., 2019), after converting FcRn concentration to content in the endosomal space (Eq (1)). The total endosomal FcRn abundance ranged from 57.2 to 126.7 μM. Reported minimal and maximal values of total lymph flow were 0.0007 and 0.0414 L/h/kg (Gill et al., 2016). The volume of the central lymph node compartment depends on the number and volume of lymph nodes in the human body. No published values were found for the boundaries of the central lymph node compartment, and thus, a 10-fold range of lymph node volume was used as the minimum to maximum boundary in the GSA. The frequency was uniform for all four parameters. The Morris method was selected, which defines the impact of a parameter by their influence on the output

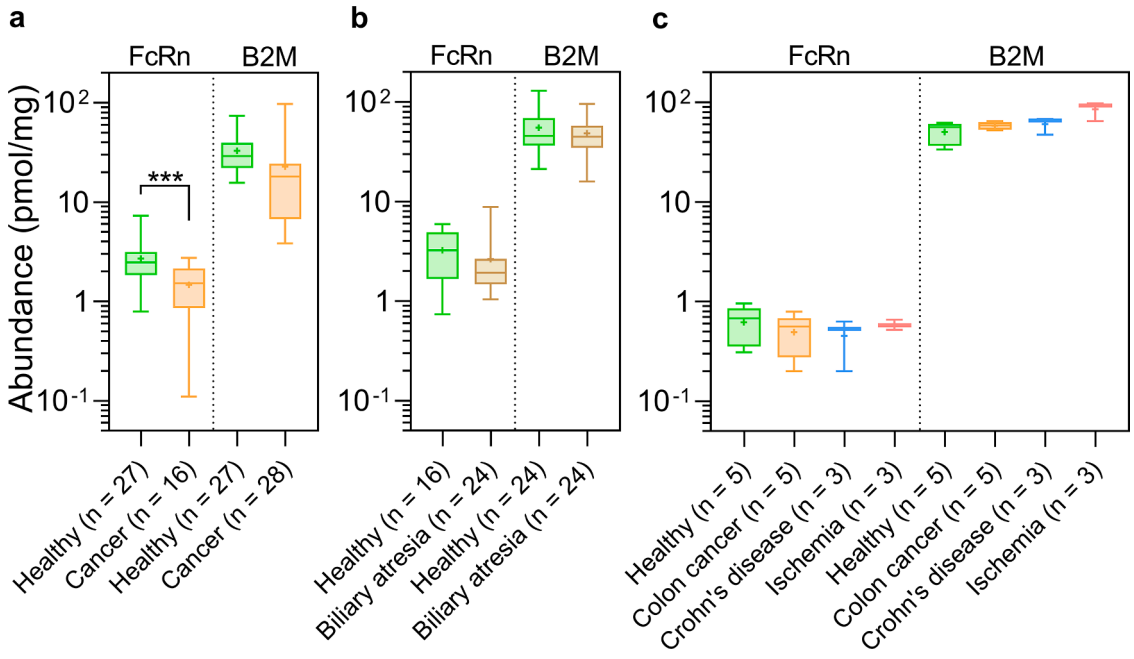

Fig. 3. Changes in protein expression of FcRn subunits p51 and B2M in liver and intestinal disease. Changes were assessed in adult liver cancer (**a**), biliary atresia in neonate and infant livers (**b**), and in intestinal diseases (**c**) relative to age-matched healthy controls. The whiskers reflect the ranges, the boxes reflect the 25th and 75th percentiles, the lines are the medians, and the + signs are the means; ***$p < 0.001$.

variable. As IV infusion was simulated, the impact on AUC rather than C_{max} or T_{max} was investigated.

3. Results

3.1. Abundance of the FcRn heterodimer in human liver, intestine, kidney and skin

The structure of the FcRn complex, formed by p51 and B2M (p14) subunits, is illustrated in Fig. 1a. The topology schematic is complemented with the amino acid sequences of the two subunits, annotated in red for peptide sequences detected by LC-MS (in this study), in gray for the transmembrane domain, in orange for the two signal peptides, and underlined font for the intra-cellular (cytosolic) domain. The quantitative distribution profile of the two subunits in liver (adult and pediatric), kidney cortex, small intestine (jejunum and ileum) and skin is presented in Fig. 1b and c. Individual abundance data are presented in Tables S1–8. Abundance is expressed in units related to the fraction in which measurements were made [picomole per mg of membrane protein (liver and kidney), picomole per mg mucosal protein (intestine) or picomole per mg post-mitochondrial supernatant protein (skin)]. A summary of abundance data is included in Table S9. Abundance data followed either normal or log-normal distribution.

3.2. Covariates of FcRn p51 and B2M expression

The expression of FcRn was assessed against several demographic and clinical factors, including sex, age, ethnicity, smoking, alcohol consumption, anatomical section and body mass index (BMI) of donors, wherever information was available. Detailed demographic and clinical information of the donors in each of the eight sets is presented in Tables S1–8.

Effect of sex. The effect of sex on FcRn abundance was assessed in the adult sets in order not to confound the impact of this variable with ontogeny-related differences (Fig. 2a). Sex of donors was available for all samples in each adult set: adult liver set 1 (15 male), adult liver set 2 (16 male), intestine (12 male), kidney (16 male), skin (1 male). There were no sex-related differences in expression of FcRn p51 subunit in adult liver, intestine or kidney (Fig. 2a). The difference in expression levels of FcRn B2M subunit between male and female donors in adult liver set 2 was of borderline significance (unpaired *t*-test, $p = 0.03$). Intestinal samples from jejunum ($n = 4$) and ileum ($n = 12$) were combined into a single set (designated as intestine) because FcRn and B2M expression was similar in the two anatomical regions (Fig. 2b).

Effect of age. Age of donors was available for all sets: adult liver set 1 (27 years–66 years), adult liver set 2 (44 years–85 years), pediatric liver set 1 (13 days–18 years), pediatric liver set 2 (fetal–7 years), pediatric liver set 3 (2 weeks–5 months), intestine (17 years–80 years), kidney (43 years–83 years) and skin (27 years–56 years). Age-related effects were investigated in non-diseased liver tissue to assess both ontogenic changes and changes after maturity. To assess ontogeny, EMA age classification was implemented to bin samples from four sets (pediatric sets 1 and 2 and adult sets 1 and 2) into fetal ($n = 5$), neonate ($n = 15$), infant ($n = 9$), child ($n = 11$), adolescent ($n = 3$) and adult ($n = 57$) groups. Differences in expression of FcRn subunits across all age bins were statistically significant (one-way ANOVA, $p = 0.02$). Abundance of FcRn p51 subunit was slightly higher in fetal (1.4 fold), neonate (1.5 fold) and infant samples (1.4 fold) relative to adult levels; differences were statistically significant in the case of neonates (post-hoc unpaired *t*-test, $p = 0.01$). Similarly, differences were observed for the B2M subunit in neonates (1.9 fold), infants (2.1 fold) and children (1.8 fold) compared with adults, with statistical significance across the three age groups (post-hoc unpaired *t*-test, $p < 0.01$). Expression of both subunits in adolescents was similar to those in adults (Fig. 2c). To assess trends of expression after maturity, adult samples from liver ($n = 57$), kidney ($n = 20$), intestine ($n = 15$) and skin ($n = 6$) were binned against age (range 18–85 years, Fig. S1). There was considerable overlap and no significant difference between adult age groups for both FcRn subunits (ANOVA and post-hoc unpaired *t*-test).

Effect of ethnicity. The effect of ethnicity was assessed in age-matched samples to avoid confounding ethnic differences with those related to ontogeny. Most of the donors were White Caucasians in all adult sets, wherever information on ethnicity was available: liver set 1 (25/27), liver set 2 (25/29), kidney set (8/20), skin set (5/6). For the rest of the donors, information on ethnicity was either not available or the other ethnic categories included only one sample each. These

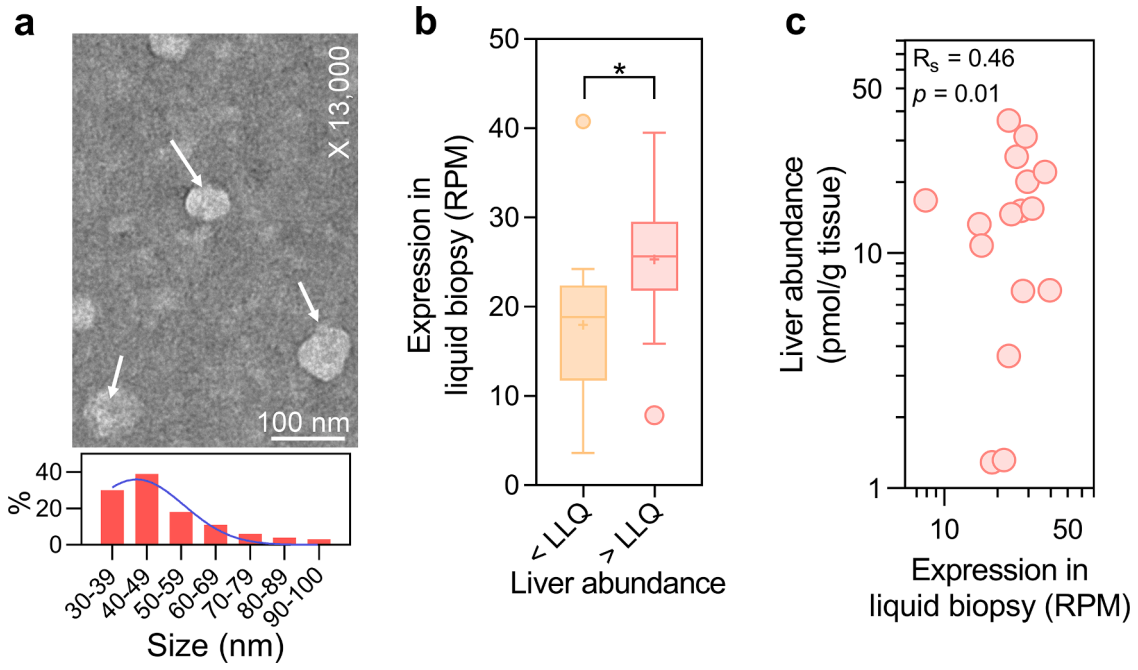

Fig. 4. Linking expression of FcRn in liver tissue with matching plasma exosomes. Exosomes (size: 30–100 nm visualized by transmission electron microscopy, X13,000) were extracted from plasma with matching liver tissue **(a)**. Higher levels of exosomal FcRn (p51 subunit) were recorded (41% difference) in donors with liver FcRn above the lower limit of quantification (LLQ) than those with hepatic FcRn below the LLQ (**b**). Moderate and statistically significant correlation was recorded between levels of FcRn in plasma exosomes and hepatic FcRn abundance in the same donors (**c**). In panel **b**, the whiskers reflect the ranges, the boxes reflect the 25th and 75th percentiles, the lines are the medians, and the + signs are the means; *$p < 0.05$. In panel **c**, correlation was assessed using Spearman's correlation coefficient (Rs). Abbreviations: LLQ, lower limit of quantification; RPM, reads per million.

categories were Asian (1 adult liver and 1 skin sample) and African American (1 adult liver). Therefore, race-related expression trends could not be investigated in adult donors. Pediatric liver set 3 was the only sample set which included a sufficient number of samples in more than one ethnic group (16 White and 7 South Asian donors). Because surgical intervention (Kasai procedure) is required for biliary atresia early in life, all 25 samples in this set originated from children of similar age (2 weeks to 5 months). This allowed assessment of the effect of ethnicity in this set, returning no differences in FcRn expression between White and Asian donors (unpaired *t*-test with Welch's correction, $p > 0.05$).

Effect of body mass index (BMI). BMI data were available for adult liver set 1 (18.0–39.8 kg/m^2), adult liver set 2 (19.5–41.7 kg/m^2) and kidney set (21.0–36.7 kg/m^2). The levels in healthy liver and kidney sets were binned into three categories: healthy BMI (18.5–25 kg/m^2), overweight (25–30 kg/m^2) and obese (>30 kg/m^2). Although mean FcRn abundance was on average 1.7- and 1.3-fold higher in liver and kidney, respectively, in overweight/obese donors compared with donors with healthy BMI, differences across the BMI range were not statistically significant (Fig. 2d). A similar trend was observed with the donors' body weight.

Effect of smoking and alcohol use. Information about smoking and alcohol use by donors was available for both adult liver sets and for the kidney set (Tables S1, S2 and S6). In adult liver set 1 ($n = 27$), six donors were smokers and 10 donors were alcohol users. The number of active smokers and alcohol users in adult liver set 2 ($n = 29$) was four and 11, respectively. Information about smoking and drinking was not available for four and 16 donors in this set, respectively. In the kidney set ($n = 20$), three donors were smokers and 11 were alcohol users. Information about smoking and drinking was not available for two and four donors in the kidney set, respectively. There was no difference in FcRn abundance in adult liver and kidney in relation to smoking or alcohol consumption (unpaired *t*-test, $p > 0.05$).

3.3. Effect of disease on FcRn p51 and B2M abundance

Adult liver set 1 ($n = 27$) and set 2 ($n = 29$) were from healthy and liver cancer donors, respectively. Pediatric liver samples were from donors with healthy liver ($n = 44$) or those with biliary atresia ($n = 25$). The intestine set included healthy donors ($n = 5$), colon cancer patients ($n = 5$), patients with ischemia ($n = 3$) or Crohn's disease ($n = 3$). The kidney samples ($n = 20$) were from cancer donors (Fig. 3). Compared with healthy adult liver, significantly lower levels of FcRn p51 (0.5 fold) were observed in histologically-normal liver adjacent to metastatic tumors (unpaired *t*-test with Welch's correction, $p < 0.001$). Levels of B2M were closer in the two sets (0.7 fold, $p > 0.05$). In the pediatric sets, age-matched samples (neonates and infants) from healthy and biliary atresia livers reflected no differences in FcRn expression ($p > 0.05$). Considering the similar expression of FcRn in jejunal and ileal samples, the effect of disease on expression was tested across all the small intestine samples, returning no significant differences (one-way ANOVA).

3.4. Inter-correlation between FcRn p51 and B2M levels

Inter-correlation of expression between FcRn subunits p51 and B2M was tested in adult liver ($n = 43$), pediatric liver ($n = 59$), kidney ($n = 20$) and intestine ($n = 16$) samples. The number of skin samples in which both subunits were quantified ($n = 4$) was too low for correlation analysis. Correlations were weak in adult and pediatric livers (Rs = 0.27–0.33, $p < 0.05$) and no correlation was recorded for kidney and intestine (Fig. S2).

3.5. Monitoring FcRn in plasma-derived exosomes

The relative concentration of FcRn mRNA in exosomes (Fig. 4a) derived from plasma samples matching tissue in adult liver set 2 was measured using RNA sequencing (Achour et al., 2021, 2022). Levels were higher (41% difference) in plasma from donors with hepatic FcRn

protein above the limit of quantification compared with donors with hepatic FcRn below the limit of quantification (*t*-test, $p = 0.03$, Fig. 4b), and a moderate correlation, with borderline significance, was recorded between plasma exosomal levels and hepatic abundance (Rs = 0.46, $p = 0.01$, Fig. 4c). Whereas a residual FcRn from other organs was recorded, contribution of the liver to the exosomal pool was significant, possibly due to high liver perfusion and therefore high tissue-to-plasma shedding, estimated at 7% (±5%) of the total shedded tissue-specific exosomal RNA from 32 organs (Fig. S3).

3.6. Simulated mAb disposition and global sensitivity analysis (GSA)

The minimal PBPK models adequately predicted trastuzumab and efalizumab pharmacokinetics following a single IV infusion (Fig. 5). The lower hepatic FcRn abundance measured in this study in cancer patients relative to healthy donors did not result in marked differences in predicted trastuzumab AUC or elimination half-life (Fig. 5a and Table 2), in line with clinical observations (Wynne et al., 2013). Rather, the PK was dependent on whether TMDD was activated in either population; simulations with TMDD predicted the AUC and $t_{1/2}$ more accurately (Table 2).

Global sensitivity analysis was used to discern the impact of various systems parameters on exposure (AUC) to IgG-based antibodies. Endogenous IgG plasma concentration was the parameter with the highest impact on the AUC (Fig. 6). FcRn had the second highest impact, with 59% lower absolute mean value than IgG. Notably, IgG concentration determines the proportion of free FcRn available for binding (and rescue) of the dosed antibody drug, which directly impacts the mAb's half-life and AUC. Lymph flow rate and central lymph node volume played a lesser role in defining exposure (90% and 97% lower absolute mean value).

4. Discussion

Quantitative systems pharmacology (QSP) models offer the possibility of detailed quantitative assessment of the pharmacology of biotherapeutics. These models are also sufficiently informative to predict the impact of disease and enable investigation of mAb targeting of specific tissues (Urva et al., 2010; Kiseleva et al., 2020). Building such models requires 'systems' data, which include the tissue-specific expression patterns of FcRn (Chetty et al., 2015). PBPK modelling suggests that IgG elimination is mainly driven by the skin, the muscles, the liver and the intestine (Tang and Meibohm, 2006), an observation which is relevant to the clearance of Fc-containing therapeutics. In this study, we provide abundance data and covariates of FcRn expression in four tissues (liver, intestine, kidneys and skin), with the aim of refining model-based predictions of the disposition of biologics.

Global proteomic data demonstrated the presence of FcRn subunits (p51 and B2M) in liver, intestine, kidney and skin, in agreement with

Table 2
Summary of predicted impact of measured changes in FcRn abundance and model settings on trastuzumab and efalizumab disposition. Predicted AUC and $t_{1/2}$ were compared to observed data (mean fold error in brackets).

		Trastuzumab: Healthy population	Trastuzumab: Cancer population	Efalizumab: Psoriasis population
Predicted – minimal PBPK model without TMDD	AUC_{inf} (μmol/L•h)	415 ± 110 (1.56)	343 ± 87 (1.15)	276 ± 81 (1.13)
	$t_{1/2}$ (h)	584 ± 280 (2.30)	521 ± 223 (2.14)	187 ± 66 (1.48)
Predicted – minimal PBPK model with TMDD	AUC_{inf} (μmol/L•h)	288 ± 80 (1.08)	244 ± 69 (0.82)	245 ± 67 (1.00)
	$t_{1/2}$ (h)	193 ± 161 (0.76)	184 ± 150 (0.75)	170 ± 63 (1.35)
Observed	AUC_{inf} (μmol/L•h)	266 ± 50	298 ± 41	244 [a]
	$t_{1/2}$ (h)	254 ± 32	244 ± 69	126 [a]

TMDD, target-mediated drug disposition (trastuzumab target: HER2; efalizumab target: CD11a); data are presented as mean ± SD; observed data from Wynne et al. (2013) and Bauer et al. (1999). [a] observed in one psoriasis patient.

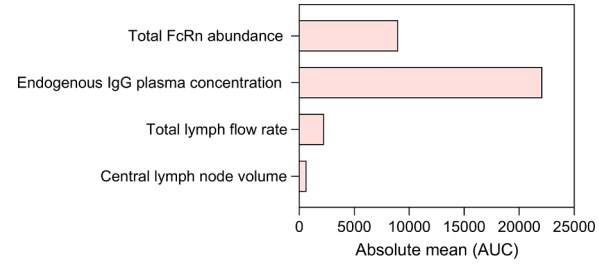

Fig. 6. Global sensitivity analysis (GSA) of the effect of four investigated systems parameters on exposure to exogenous IgG-based antibodies in a minimal PBPK model. The highest impact was observed with endogenous IgG concentration and FcRn abundance.

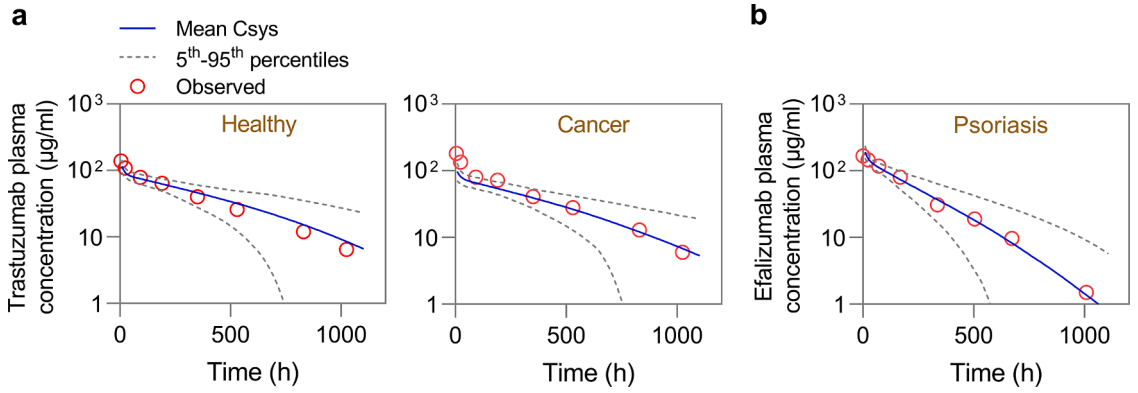

Fig. 5. Predicted plasma concentration profiles of trastuzumab (a) and efalizumab (b) after a single IV infusion in healthy and cancer populations (trastuzumab) and a psoriasis population (efalizumab). Observed data for healthy volunteers, cancer patients and psoriasis patients (red circles) were from (Wynne et al., 2013; Bauer et al., 1999). The solid and the dashed lines show the predicted mean systemic mAb concentration (Csys) and the 5th–95th percentiles for the simulated virtual populations. The models used target-mediated drug disposition (TMDD) with HER2 as the drug target of trastuzumab and CD11a as the target of efalizumab. Predicted differences between healthy volunteers and patients were in line with the clinical data. Observed data were generated by immunoquantification (Wynne et al., 2013; Bauer et al., 1999).

Fan et al. (2019), who investigated FcRn expression in 14 tissues, from 5 donors each, using targeted proteomics. Our study provides data in a larger sample set (6–69 donors per tissue set), offering a more realistic measure of inter-individual variability in the four tissues. A more recent study (Qiu and Wang, 2020) also used targeted proteomics to measure FcRn in 39 donors, focusing only on liver. Head-to-head comparison of FcRn p51 abundance in the present study and those in the previous two studies (Fan et al., 2019; Qiu and Wang, 2020) required scaling to tissue content. For healthy liver, scaling our abundance measurements using MPPGL data (40.7 ± 10.9 mg/g liver), generated in-house (El-Khateeb et al., 2020), returned levels comparable to those previously reported [mean FcRn abundance of 110.1 pmol/g liver, compared with 89.5 pmol/g (Fan et al., 2019) and 147 pmol/g (Qiu and Wang, 2020)]. Likewise, kidney levels were scaled up using in-house MPPGK data [26.2 ± 7.1 mg/g kidney cortex (Scotcher et al., 2017)], which returned tissue levels comparable to those reported [mean FcRn abundance of 37.6 pmol/g of kidney cortex compared with 48.3 pmol/g (Fan et al., 2019)]. Compared with expression in liver and kidney, lower FcRn abundance was observed in intestine and skin preparations, and levels in brain samples ($n = 22$) (Al-Majdoub et al., 2019, 2020) were below the limit of detection. FcRn mRNA levels in the brain were previously reported to be very low (Fagerberg et al., 2014), and previous proteomic measurements in tissue (Fan et al., 2019) suggested lower levels in kidney, intestine, skin and brain compared with liver.

Abundance of the B2M subunit was reported previously in adult liver at approximately one order of magnitude (8.5 fold) higher than FcRn p51 subunit (mean abundance of 1248 pmol/g tissue) (Qiu and Wang, 2020). Our data are in agreement with this finding (12.1 fold, scaled mean abundance 1539 pmol/g tissue), and we add B2M abundance data in pediatric liver (19.4 fold), intestine (112.8 fold), kidney (46.3 fold) and skin (36.3 fold). These findings are supported by mRNA evidence, estimating B2M levels at 6 to 26-fold higher than FcRn p51 in the four tissues under investigation (Fagerberg et al., 2014). The observation of higher B2M levels is not surprising; B2M participates in the structure of other MHC class I molecules (Burmeister et al., 1994; Story et al., 1994). Functionally, B2M is speculated to be involved in cell surface expression of FcRn and facilitating ligand binding to endogenous IgG (Praetor and Hunziker, 2002) and, by extension, Fc-containing biologics. Correlating abundance of the two subunits in liver, intestine and kidney revealed a weak correlation only in liver, which is in agreement with recent findings by Qiu and Wang (2020).

A novel finding of this study is the assessment of covariates of FcRn expression with reference to demographic and clinical information. One of the highlights of this assessment was the lack of difference in expression (in liver, kidney and intestine) with sex and age after maturity. The lack of effect of sex and age on expression was previously reported only in adult liver (Qiu and Wang, 2020). More importantly, we investigated ontogenic development in liver (where the age of donors covered a wide developmental age range). We uncovered, for the first time, a declining trend in abundance, especially from neonatal to adult levels, which was predicted previously by a minimal PBPK model of IgG and bevacizumab (Hardiansyah and Ng, 2018). A similar trend of declining (neonatal to adult) levels was observed in rat intestine using mRNA data (Martín et al., 1997). In addition, we observed a lack of differential expression between jejunum and ileum, in line with mRNA data in small intestinal segments of rodent and primate preclinical species (Lawrence et al., 2021). These findings (ontogenic and regional trends) should be confirmed at the tissue level as the amount of fraction protein per gram tissue also contributes to differences in protein expression in tissue (Leeder et al., 2022; Harwood et al., 2013).

Annotation with clinical data revealed down-regulation of FcRn p51 subunit (encoded by the FCGRT gene) in histologically normal liver tissue adjacent to tumor compared with healthy liver. Consistent with the suppressive effect of the cancer microenvironment, lower expression of the FCGRT gene was previously reported in progressive breast carcinoma (Jansen et al., 2005), non-small cell lung cancer (Dalloneau et al., 2016) and hepatocellular carcinoma (Shi et al., 2016), associated in all cases with poor prognosis (Cadena Castaneda et al., 2020). It is not clear, however, in which type of cells in the liver the measured FcRn abundance has changed. If this happened in the endothelial cells, transcytosis flux may decline but this pathway of extravasation is likely to be negligible even under normal physiological conditions. This leaves the question of whether FcRn suppression in 'normal' liver tissue represents downregulation in some or all of the different cell types, i.e., Kupfer cells and/or hepatocytes, or replacement of cells with fibroblasts, following cytotoxic treatment with chemotherapy. Further, lumping FcRn abundance in the endosomal compartment within a minimal PBPK model "masked" the effects of differences in FcRn observed in one single tissue (liver) on the elimination half-life. The liver is responsible for ~30% of IgG degradation (Eigenmann et al., 2017), and thus, the effect of reduced hepatic FcRn abundance is expected to be more discernible in a full PBPK model. However, the magnitude of the effect reported *in vivo* for trastuzumab was not significant (Wynne et al., 2013).

A trend of increased FcRn expression in liver with BMI is suggested by the data, which may be associated with previously reported accumulation of macrophages in obesity to maintain IgG homeostasis (Challa et al., 2019). Of interest, the measured FcRn tendencies match those observed for IgG in relation to sex and BMI (Gonzalez-Quintela et al., 2008). This observation is supported by the global sensitivity analysis done with a PBPK model of a mAb; endogenous IgG plasma concentration was the systems parameter with the highest impact on AUC followed by FcRn abundance. At steady state, approximately half of the dosed mAb (and endogenous IgG) is found in the central plasma compartment, while the rest is extravascular, flowing through interstitial space and the lymphatic system (Betts et al., 2018). The endogenous IgG and the exogenous mAb compete for FcRn binding, and therefore, the higher the IgG concentration the higher the degradation of the mAb, which explains most of the estimated sensitivity. Both parameters were demonstrated by modelling to influence antibody clearance (Li et al., 2014). Importantly, the impact of endogenous IgG and FcRn abundance depends also on the endocytosis rate and the binding affinity of the investigated mAb to FcRn. In addition, endogenous IgG plasma concentration can only be a surrogate for the steady-state concentration in the endosomal space that will affect the pharmacokinetics of a mAb. The endosomal volume is not well characterized and will also have an impact on endosomal concentrations as well as the free endosomal mAb degradation rate, which was not the focus of the current analysis.

A limitation to individualization of systems-informed models, such as the ones described in this study, is the requirement for invasive tissue samples. A less invasive alternative may be offered by exosome-based liquid biopsies. Although not perfect, the quantitative link between liver tissue and plasma exosomal levels of FcRn demonstrated herein for the first time is encouraging. This supports recent findings that advocate the use of data from liquid biopsy (Achour et al., 2021, 2022) for the creation and implementation of virtual twins of patients with the aim of supporting personalized therapeutics (Polasek and Rostami-Hodjegan, 2020; Darwich et al., 2021).

5. Conclusions

Quantitative proteomics offered unique insights into the distribution and abundance of the FcRn receptor, valuable for the prediction of the disposition and effect of biotherapeutics. The patterns of expression reported here, with reference to clinical and demographic characteristics, have the potential to further refine the performance of biologics modelling platforms. A quantitative link between tissue and plasma exosomes adds more value to the use of liquid biopsy for personalization of QSP models. We consider these findings as initial steps toward rationalizing the use of more mechanistic models for biologics, and we look forward to further integration of such data in the evaluation of existing and new therapeutic biomolecules.

Data availability

The proteomic data are available on the Proteomics Identifications (PRIDE) repository with the dataset identifiers: PXD020910 (adult liver set 1), PXD021025 (adult liver set 2), PXD020844 (pediatric liver set 1), PXD020939 (pediatric liver set 2), PXD020974 (pediatric liver set 3), PXD020996 (kidney), PXD020987 (intestine) and PXD020742 (skin).

CRediT authorship contribution statement

Jill Barber: Data curation, Supervision, Funding acquisition, Writing – review & editing. **Zubida M. Al-Majdoub:** Data curation, Investigation, Writing – review & editing. **Narciso Couto:** Investigation. **Martyn Howard:** Investigation. **Yasmine Elmorsi:** Investigation. **Daniel Scotcher:** Investigation, Writing – review & editing. **Naved Alizai:** Resources, Writing – review & editing. **Saskia de Wildt:** Resources, Writing – review & editing. **Felix Stader:** Conceptualization, Software, Writing – review & editing. **Armin Sepp:** Conceptualization, Formal analysis, Software, Writing – review & editing. **Amin Rostami-Hodjegan:** Conceptualization, Supervision, Funding acquisition, Writing – review & editing. **Brahim Achour:** Conceptualization, Supervision, Funding acquisition, Investigation, Data curation, Formal analysis, Visualization, Project administration, Software, Writing – original draft.

Declaration of Competing Interest

Felix Stader, Armin Sepp and Amin Rostami-Hodjegan are employees of Certara Ltd., a provider of modelling and simulation platforms in the quantitative systems pharmacology space to academic and industrial institutions. The other authors declare no competing interests.

Data availability

Data are available on a public repository (PRIDE) as described in the manuscript.

Acknowledgements

The authors acknowledge support from the CAPKR consortium funded by Janssen, Takeda, MSD, Eli Lilly, Genentech, GSK, AbbVie and Servier. The authors thank the Biological Mass Spectrometry Core Facility (BioMS), University of Manchester, and the ChELSI Institute, University of Sheffield, for access to LC-MS instrumentation, and Illumina for access to sequencing facilities. We also thank Pfizer (liver tissue fractions), Manchester Biomedical Research center (BRC) Biobank, University of Manchester (adult liver and kidney samples), Sekisui XenoTech, Invitron, Erasmus University Medical center and Ethical Tissue University of Bradford Biobank (pediatric liver samples), Salford Royal NHS Foundation Trust (intestine samples) and Bradford University Teaching Hospital (skin samples).

Supplementary materials

Supplementary material associated with this article can be found, in the online version, at doi:10.1016/j.ejps.2023.106375.

References

Achour, B., Al-Majdoub, Z.M., Grybos-Gajniak, A., Lea, K., Kilford, P., Zhang, M., Knight, D., Barber, J., Schageman, J., Rostami-Hodjegan, A., 2021. Liquid biopsy enables quantification of the abundance and interindividual variability of hepatic enzymes and transporters. Clin. Pharmacol. Ther. 109, 222–232.

Achour, B., Gosselin, P., Terrier, J., Gloor, Y., Al-Majdoub, Z.M., Polasek, T.M., Daali, Y., Rostami-Hodjegan, A., Reny, J., 2022. Liquid biopsy for patient characterization in cardiovascular disease: verification against markers of cytochrome P450 and P-glycoprotein activities. Clin. Pharmacol. Ther. 111, 1268–1277.

Al Feteisi, H., Al-Majdoub, Z.M., Achour, B., Couto, N., Rostami-Hodjegan, A., Barber, J., 2018. Identification and quantification of blood-brain barrier transporters in isolated rat brain microvessels. J. Neurochem. 146, 670–685.

Al-Majdoub, Z.M., Carroll, K.M., Gaskell, S.J., Barber, J., 2014. Quantification of the proteins of the bacterial ribosome using QconCAT technology. J. Proteome Res. 13, 1211–1222.

Al-Majdoub, Z.M., Achour, B., Couto, N., Howard, M., Elmorsi, Y., Scotcher, D., Alrubia, S., El-Khateeb, E., Vasilogianni, A.-.M., Alohali, N., Neuhoff, S., Schmitt, L., Rostami-Hodjegan, A., Barber, J., 2020. Mass spectrometry-based abundance atlas of ABC transporters in human liver, gut, kidney, brain and skin. FEBS Lett. 594, 4134–4150.

Al-Majdoub, Z.M., Al Feteisi, H., Achour, B., Warwood, S., Neuhoff, S., Rostami-Hodjegan, A., Barber, J., 2019. Proteomic quantification of human blood–brain barrier SLC and ABC transporters in healthy individuals and dementia patients. Mol. Pharm. 16, 1220–1233.

Al-Majdoub, Z.M., Couto, N., Achour, B., Harwood, M.D., Carlson, G., Warhurst, G., Barber, J., Rostami-Hodjegan, A., 2021a. Quantification of proteins involved in intestinal epithelial handling of xenobiotics. Clin. Pharmacol. Ther. 109, 1136–1146.

Al-Majdoub, Z.M., Scotcher, D., Achour, B., Barber, J., Galetin, A., Rostami-Hodjegan, A., 2021b. Quantitative proteomic map of enzymes and transporters in the human kidney: stepping closer to mechanistic kidney models to define local kinetics. Clin. Pharmacol. Ther. 110, 1389–1400.

Bauer, R.J., Dedrick, R.L., White, M.L., Murray, M.J., Garovoy, M.R., 1999. Population pharmacokinetics and pharmacodynamics of the anti-CD11a antibody hu1124 in human subjects with psoriasis. J. Pharmacokinet. Biopharm. 27, 397–420.

Betts, A., Keunecke, A., van Steeg, T.J., van der Graaf, P.H., Avery, L.B., Jones, H., Berkhout, J., 2018. Linear pharmacokinetic parameters for monoclonal antibodies are similar within a species and across different pharmacological targets: a comparison between human, cynomolgus monkey and hFcRn Tg32 transgenic mouse using a population-modeling approach. MAbs 10, 751–764.

Burmeister, W.P., Gastinel, L.N., Simister, N.E., Blum, M.L., Bjorkman, P.J., 1994. Crystal structure at 2.2Å resolution of the MHC-related neonatal Fc receptor. Nature 372, 336–343.

Cadena Castaneda, D., Brachet, G., Goupille, C., Ouldamer, L., Gouilleux-Gruart, V., 2020. The neonatal Fc receptor in cancer FcRn in cancer. Cancer Med. 9, 4736–4742.

Challa, D.K., Wang, X., Montoyo, H.P., Velmurugan, R., Ober, R.J., Ward, E.S., 2019. Neonatal Fc receptor expression in macrophages is indispensable for IgG homeostasis. MAbs 11, 848–860.

Chang, H.-.P., Kim, S.J., Shah, D.K., 2021. Whole-body pharmacokinetics of antibody in mice determined using enzyme-linked immunosorbent assay and derivation of tissue interstitial concentrations. J. Pharm. Sci. 110, 446–457.

Chetty, M., Li, L., Rose, R., Machavaram, K., Jamei, M., Rostami-Hodjegan, A., Gardner, I., 2015. Prediction of the pharmacokinetics, pharmacodynamics, and efficacy of a monoclonal antibody, using a physiologically based pharmacokinetic FcRn model. Front. Immunol. 5, 670.

Couto, N., Al-Majdoub, Z.M., Achour, B., Wright, P.C., Rostami-Hodjegan, A., Barber, J., 2019. Quantification of proteins involved in drug metabolism and disposition in the human liver using label-free global proteomics. Mol. Pharm. 16, 632–647.

Couto, N., Al-Majdoub, Z.M., Gibson, S., Davies, P.J., Achour, B., Harwood, M.D., Carlson, G., Barber, J., Rostami-Hodjegan, A., Warhurst, G., 2020. Quantitative proteomics of clinically relevant drug-metabolizing enzymes and drug transporters and their intercorrelations in the human small intestine. Drug Metab. Dispos. 48, 245–254.

Couto, N., Newton, J.R.A., Russo, C., Karunakaran, E., Achour, B., Al-Majdoub, Z.M., Sidaway, J., Rostami-Hodjegan, A., Clench, M.R., Barber, J., 2021. Label-free quantitative proteomics and substrate-based mass spectrometry imaging of xenobiotic metabolizing enzymes in *ex vivo* human skin and a human living skin equivalent model. Drug Metab. Dispos. 49, 39–52.

Dalloneau, E., Baroukh, N., Mavridis, K., Maillet, A., Gueugnon, F., Courty, Y., Petit, A., Kryza, T., Del Rio, M., Guyetant, S., Cadena Castaneda, D.C., Dhommée, C., Arnoult, C., Scorilas, A., Gouilleux-Gruart, V., Heuzé-Vourc'h, N., 2016. Downregulation of the neonatal Fc receptor expression in non-small cell lung cancer tissue is associated with a poor prognosis. Oncotarget 7, 54415–54429.

Darwich, A.S., Polasek, T.M., Aronson, J.K., Ogungbenro, K., Wright, D.F., Achour, B., Reny, J.L., Daali, Y., Eiermann, B., Cook, J., Lesko, L., McLachlan, A.J., Rostami-Hodjegan, A., 2021. Model-informed precision dosing: background, requirements, validation, implementation, and forward trajectory of individualizing drug therapy. Ann. Rev. Pharmacol. Toxicol. 61, 225–245.

Dostalek, M., Gardner, I., Gurbaxani, B.M., Rose, R.H., Chetty, M., 2013. Pharmacokinetics, pharmacodynamics and physiologically-based pharmacokinetic modelling of monoclonal antibodies. Clin. Pharmacokinet. 52, 83–124.

Eigenmann, M.J., Fronton, L., Grimm, H.P., Otteneder, M.B., Krippendorff, B.F., 2017. Quantification of IgG monoclonal antibody clearance in tissues. MAbs 9, 1007–1015, 2017.

El-Khateeb, E., Achour, B., Scotcher, D., Al-Majdoub, Z.M., Athwal, V., Barber, J., Rostami-Hodjegan, A., 2020. Scaling factors for clearance in adult liver cirrhosis. Drug Metab. Dispos. 48, 1271–1282.

Fagerberg, L., Hallström, B.M., Oksvold, P., Kampf, C., Djureinovic, D., Odeberg, J., Habuka, M., Tahmasebpoor, S., Danielsson, A., Edlund, K., Asplund, A., Sjöstedt, E., Lundberg, E., Szigyarto, C.A.-.K., Skogs, M., Takanen, J.O., Berling, H., Tegel, H., Mulder, J., Nilsson, P., Schwenk, J.M., Lindskog, C., Danielsson, F., Mardinoglu, A., Sivertsson, A., von Feilitzen, K., Forsberg, M., Zwahlen, M., Olsson, I., Navani, S., Huss, M., Nielsen, J., Ponten, F., Uhlén, M., 2014. Analysis of the human tissue-

specific expression by genome-wide integration of transcriptomics and antibody-based proteomics. Mol. Cell. Proteomics 13, 397–406.
Fan, Y.Y., Farrokhi, V., Caiazzo, T., Wang, M., O'Hara, D.M., Neubert, H., 2019. Human FcRn tissue expression profile and half-life in PBMCs. Biomolecules 9, 373.
Food and Drug Administration (2020) Enhancing the diversity of clinical trial populations – eligibility criteria, enrollment practices, and trial designs, Guidance for Industry. Available from: https://www.fda.gov/regulatory-information/search-fda-guidance-documents/enhancing-diversity-clinical-trial-populations-eligibility-criteria-enrollment-practices-and-trial.
Food and Drug Administration (2022), Diversity plans to improve enrollment of participants from underrepresented racial and ethnic populations in clinical trials, Draft Guidance for Industry, (2022). Available from: https://www.fda.gov/regulatory-information/search-fda-guidance-documents/diversity-plans-improve-enrollment-participants-underrepresented-racial-and-ethnic-populations.
Gill, K.L., Gardner, I., Li, L., Jamei, M., 2016. A bottom-up whole-body physiologically based pharmacokinetic model to mechanistically predict tissue distribution and the rate of subcutaneous absorption of therapeutic proteins. AAPS J. 18, 156–170.
Gonzalez-Quintela, A., Alende, R., Gude, F., Campos, J., Rey, J., Meijide, L.M., Fernandez-Merino, C., Vidal, C., 2008. Serum levels of immunoglobulins (IgG, IgA, IgM) in a general adult population and their relationship with alcohol consumption, smoking and common metabolic abnormalities. Clin. Exp. Immunol. 151, 42–50.
Hardiansyah, D., Ng, C.M., 2018. Effects of the FcRn developmental pharmacology on the pharmacokinetics of therapeutic monoclonal IgG antibody in pediatric subjects using minimal physiologically-based pharmacokinetic modelling. MAbs 10, 1144–1156.
Harwood, M.D., Neuhoff, S., Carlson, G.L., Warhurst, G., Rostami-Hodjegan, A., 2013. Absolute abundance and function of intestinal drug transporters: a prerequisite for fully mechanistic *in vitro-in vivo* extrapolation of oral drug absorption. Biopharm. Drug Dispos. 34, 2–28.
Jansen, M.P.H.M., Foekens, J.A., van Staveren, I.L., Dirkzwager-Kiel, M.M., Ritstier, K., Look, M.P., Meijer-van Gelder, M.E., Sieuwerts, A.M., Portengen, H., Dorssers, L.C.J., Klijn, J.G.M., Berns, E.M.J.J., 2005. Molecular classification of tamoxifen-resistant breast carcinomas by gene expression profiling. J. Clin. Oncol. 23, 732–740.
Kiseleva, RYu, Glassman, P.G., LeForte, K.M., Walsh, L.R., Villa, C.H., Shuvaev, V.V., Myerson, J.W., Aprelev, P.A., Marcos-Contreras, O.A., Muzykantov, V.R., Greineder, C.F., 2020. Bivalent engagement of endothelial surface antigens is critical to prolonged surface targeting and protein delivery *in vivo*. FASEB J. 34, 11577–11593.
Lawrence, S.A., Blankenship, R., Brown, R., Estwick, S., Ellis, B., Thangaraju, A., Datta-Mannan, A., 2021. Influence of FcRn binding properties on the gastrointestinal absorption and exposure profile of Fc molecules. Bioorg. Med. Chem. 32, 115942.
Leeder, J.S., Dinh, J.C., Gaedigk, A., Staggs, V.S., Prasad, B., Pearce, R.E., 2022. Ontogeny of scaling factors for pediatric physiology-based pharmacokinetic modeling and simulation: microsomal protein per gram of liver. Drug Metab. Dispos. 50, 24–32.
Li, L., Gardner, I., Dostalek, M., Jamei, M., 2014. Simulation of monoclonal antibody pharmacokinetics in humans using a minimal physiologically based model. AAPS J. 16, 1097–1109.
Martín, M.G., Wu, S.V., Walsh, J.H., 1997. Ontogenetic development and distribution of antibody transport and Fc receptor mRNA expression in rat intestine. Dig. Dis. Sci. 42, 1062–1069.
Polasek, T.M., Rostami-Hodjegan, A., 2020. Virtual twins: understanding the data required for model-informed precision dosing. Clin. Pharmacol. Ther. 107, 742–745.
Praetor, A., Hunziker, W., 2002. β2-microglobulin is important for cell surface expression and pH-dependent IgG binding of human FcRn. J. Cell Sci. 115, 2389–2397.
Pyzik, M., Sand, K.M.K., Hubbard, J.J., Andersen, J.T., Sandlie, I., Blumberg, R.S., 2019. The neonatal Fc receptor (FcRn): a misnomer? Front. Immunol. 10, 1540.
Qiu, X., Wang, M.Z., 2020. Quantification of neonatal Fc receptor and beta-2 microglobulin in human liver tissues by ultraperformance liquid chromatography–multiple reaction monitoring–based targeted quantitative proteomics for applications in biotherapeutic physiologically-based pharmacokinetic models. Drug Metab. Dispos. 48, 925–933.
Roopenian, D.C., Akilesh, S., 2007. FcRn: the neonatal Fc receptor comes of age. Nat. Rev. Immunol. 7, 715–725.
Rostami-Hodjegan, A., Achour, B., 2022. On the verge of impossibility: accounting for variability arising from permutations of comorbidities that affect the fate of drugs in the human body. In: Macheras, P (Ed.), Advances in Pharmacokinetics and Pharmacodynamics. Springer-Nature, New York.
Russell, M.R., Achour, B., McKenzie, E.A., Lopez, R., Harwood, M.D., Rostami-Hodjegan, A., Barber, J., 2013. Alternative fusion protein strategies to express recalcitrant QconCAT proteins for quantitative proteomics of human drug metabolizing enzymes and transporters. J. Proteome Res. 12, 5934–5942.
Scotcher, D., Billington, S., Brown, J., Jones, C.R., Brown, C.D.A.A., Rostami-Hodjegan, A., Galetin, A., 2017. Microsomal and cytosolic scaling factors in dog and human kidney cortex and application for *in vitro-in vivo* extrapolation of renal metabolic clearance. Drug Metab. Dispos. 45, 556–568.
Shi, L., Zhang, W., Zou, F., Mei, L., Wu, G., Teng, Y., 2016. KLHL21, a novel gene that contributes to the progression of hepatocellular carcinoma. BMC Cancer 16, 815.
Shi, S., 2014. Biologics: an update and challenge of their pharmacokinetics. Curr. Drug Metab. 15, 271–290.
Simister, N.E., Rees, A.R., 1985. Isolation and characterization of an Fc receptor from neonatal rat small intestine. Eur. J. Immunol. 15, 733–738.
Spiekermann, G.M., Finn, P.W., Ward, E.S., Dumont, J., Dickinson, B.L., Blumberg, R.S., Lencer, W.I., 2002. Receptor-mediated Immunoglobulin G Transport Across Mucosal Barriers in Adult Life. J. Exp. Med. 196, 303–310.
Story, C.M., Mikulska, J.E., Simister, N.E., 1994. A major histocompatibility complex class I-like Fc receptor cloned from human placenta: possible role in transfer of immunoglobulin G from mother to fetus. J. Exp. Med. 180, 2377–2381.
Tang, L., Meibohm, B., 2006. Pharmacokinetics of Peptides and Proteins. Pharmacokinetics and Pharmacodynamics of Biotech Drugs. Wiley-VCH Verlag GmbH & Co. KGaA, Weinheim, Germany, pp. 15–43.
Urva, S.R., Yang, V.C., Balthasar, J.P., 2010. Physiologically based pharmacokinetic model for T84.66: a monoclonal anti-CEA antibody. J. Pharm. Sci. 99, 1582–1600.
Vasilogianni, A.-.M., El-Khateeb, E., Al-Majdoub, Z.M., Alrubia, S., Rostami-Hodjegan, A., Barber, J., Achour, B., 2022. Proteomic quantification of perturbation to pharmacokinetic target proteins in liver disease. J. Proteom. 263, 104601.
Wiśniewski, J.R., Hein, M.Y., Cox, J., Mann, M., 2014. A "proteomic ruler" for protein copy number and concentration estimation without spike-in standards. Mol. Cell. Proteom. 13, 3497–3506.
Wiśniewski, J.R., Zougman, A., Nagaraj, N., Mann, M., 2009. Universal sample preparation method for proteome analysis. Nat. Methods 6, 359–362.
Wynne, C., Harvey, V., Schwabe, C., Waaka, D., McIntyre, C., Bittner, B., 2013. Comparison of subcutaneous and intravenous administration of trastuzumab: a Phase I/Ib trial in healthy male volunteers and patients with HER2-positive breast cancer. J. Clin. Pharmacol. 53, 192–201.
Xiao, J.J., 2012. Pharmacokinetic models for FcRn-mediated IgG disposition. J. Biomed. Biotechnol. 2012, 282989.